

Coulomb screening and electronic instabilities of small-diameter (5,0) nanotubes

J. González¹ and E. Perfetto^{1,2}

¹*Instituto de Estructura de la Materia. Consejo Superior de Investigaciones Científicas. Serrano 123, 28006 Madrid. Spain.*

²*Istituto Nazionale di Fisica Nucleare - Laboratori Nazionali di Frascati, Via E. Fermi 40, 00044 Frascati, Italy.*

(Dated: July 10, 2021)

We investigate the instabilities that may lead to the breakdown of the Luttinger liquid in the small-diameter (5,0) nanotubes, paying attention to the competition between the effective interaction mediated by phonon-exchange and the Coulomb interaction. We use bosonization methods to achieve an exact treatment of the Coulomb interaction at small momentum-transfer, and apply next renormalization group methods to analyze the low-energy behavior of the electron system. This allows us to discern the growth of several response functions for charge-density-wave modulations and for superconducting instabilities with different order parameters. We show that, in the case of single nanotubes exposed to screening by external gates, the Luttinger liquid is unstable against the onset of a strong-coupling phase with very large charge-density-wave correlations. The temperature of crossover to the new phase depends crucially on the dielectric constant κ of the environment, ranging from $T_c \sim 10^{-4}$ K (at $\kappa \approx 1$) up to a value $T_c \sim 10^2$ K (reached from $\kappa \approx 10$). The physical picture is however different when we consider the case of a large array of nanotubes, in which there is a three-dimensional screening of the Coulomb interaction over distances much larger than the intertube separation. The electronic instability is then triggered by the divergence of one of the charge stiffnesses in the Luttinger liquid, implying a divergent compressibility and the appearance of a regime of phase separation into spatial regions with excess and defect of electron density.

I. INTRODUCTION

During the last decade, carbon nanotubes have shown a great potential for the development of molecular electronics. This comes from their versatile electronic properties, which depend on variables like the helicity of the tubule, the temperature, or the contacts used in the experiments. It is well-known for instance that the carbon nanotubes may have semiconducting or metallic behavior, depending on the roll-up direction of the wrapped hexagonal carbon lattice¹. This has opened the way for the construction of intramolecular junctions behaving as electronic devices at the nanometer scale².

Given their reduced dimensionality, the metallic nanotubes behave as strongly correlated electron systems, with different regimes depending on the energy scale. At room temperature, for instance, the strong Coulomb repulsion prevails in nanotubes of typical radius, driving the electron system to a state with the properties of the so-called Luttinger liquid, characterized by the absence of electron quasiparticles at the Fermi level. This feature manifests in the power-law dependence of observables such as the tunnelling density of states, whose suppression at low energies has been actually observed in measurements of the conductance in the carbon nanotubes^{2,3}.

At low temperatures, the behavior of the carbon nanotubes depends on the contacts used in the transport measurements. When the contacts are not highly transparent, there is in general a suppression of the zero-bias conductance and the differential conductivity, charac-

teristic of the Coulomb blockade regime. On the other hand, there have been experiments using high-quality contacts where it has been possible to observe superconducting correlations in the carbon nanotubes^{4,5}. The most remarkable signature has been the appearance of supercurrents in nanotube ropes suspended between superconducting electrodes⁴. This feature may be understood as a consequence of the proximity effect, by which Cooper pairs are formed in the nanotubes near the superconducting electrodes⁶. Moreover, superconducting transitions have been measured in ropes suspended between metallic, nonsuperconducting electrodes^{7,8}. These observations imply the existence of a regime with a relevant attractive component in the electron-electron interaction, coming presumably from the exchange of phonons between electronic currents⁹.

¿From a theoretical point of view, it is well-known that the Luttinger liquid regime may break down in the carbon nanotubes, due to a variety of low-temperature instabilities^{10,11,12,13,14}. When the effective phonon-mediated interactions are taken into account, it can be shown that the superconducting correlations may grow large upon suitable screening of the Coulomb interaction in the nanotubes¹⁵. This has raised the hopes that such correlations could be amplified by considering nanotube geometries with enhanced electron-phonon couplings. The case of the small-diameter nanotubes, with radius down to 0.2 nm, is particularly interesting in that respect, since the large curvature of the tubule increases significantly the coupling to the elastic modes of the nanotube lattice^{16,17}.

The transport properties of small-diameter nanotubes have been studied in the experiment reported in Ref. 18, where it has been claimed evidence for a superconducting transition at about 15 K. It is uncertain however

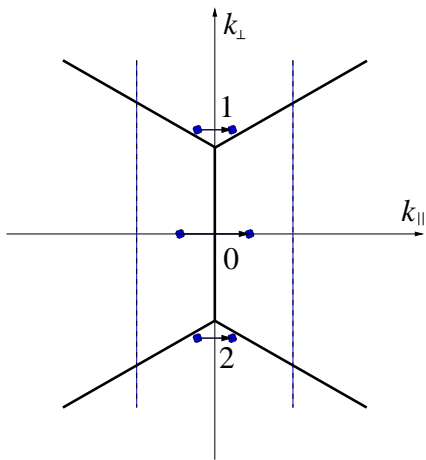


FIG. 1: Representation of the Brillouin zone of the (5,0) nanotubes showing the position of the Fermi points belonging to the low-energy degenerate subbands (denoted by 1,2) and to the zero angular-momentum subband (denoted by 0).

whether the observed features should be ascribed to the presence of nanotubes with the (5,0) or the (3,3) geometry, both being consistent with the measured nanotube radius. Moreover, it remains also unclear the physical meaning of the estimated transition temperature, as the nanotubes in the experiment are placed in the channels of a zeolite matrix that does not allow coherent electron hopping between the nanotubes.

The aim of the present paper is to investigate the instabilities that may lead to the breakdown of the Luttinger liquid in the small-diameter zig-zag nanotubes. We are going to focus on the analysis of the (5,0) nanotubes, which deserve special attention as they have three subbands crossing the Fermi level (in the undoped system). The position of the different Fermi points in momentum space is shown in Fig. 1. They correspond to two degenerate subbands with opposite values of the angular momentum around the nanotube axis (denoted by 1,2) and a third subband with zero angular momentum (labelled by 0 in the figure). The Fermi velocity is different in the nondegenerate and the degenerate subbands, being smaller in either case than for nanotubes of normal radius and leading to an enhanced density of states at low energies. For the degenerate subbands, the Fermi velocity becomes $v_F \approx 2.8 \times 10^5 \text{ ms}^{-1}$, while for the nondegenerate subband we have $v_F^{(0)} \approx 6.9 \times 10^5 \text{ ms}^{-1}$. A diagram with the different shapes of the subbands along the momentum in the longitudinal direction is shown in Fig. 2.

Together with the enhanced density of states at low energies, the large curvature of the tubule makes the (5,0) geometry the most appealing instance to study the effects of large electronic correlations in the carbon nanotubes. We will apply renormalization group methods¹⁹ to discern the low-energy instabilities of the electron system with three subbands at the Fermi level, extending the

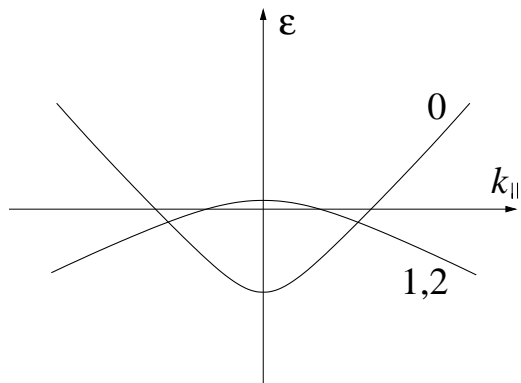


FIG. 2: Schematic representation of the dispersion of the low-energy degenerate subbands (superposed in the curve labelled by 1 and 2) and the zero angular-momentum subband (labelled by 0) of the (5,0) nanotubes. The Fermi level corresponds to $\epsilon = 0$ (in the undoped system).

analysis carried out in Refs. 11 and 20 for typical nanotubes with two low-energy subbands. This will allow us to study the growth of several response functions marking the tendency towards long-range order, including charge-density-wave (CDW) modulations with different values of the momentum and superconducting instabilities with different order parameters.

Our analysis will stress the relevance that the screening of the Coulomb interaction has for the development of different instabilities in the small-diameter nanotubes. For a single nanotube, placed in general above some substrate, there is little reduction of the Coulomb potential, which remains long-ranged in the one-dimensional (1D) system²¹. The Coulomb interaction has then a strong effective coupling, much larger than that of the effective phonon-mediated interaction, so that the Coulomb repulsion plays the dominant role dictating the electronic properties about room temperatures. We will use bosonization methods²² to achieve an exact treatment of the contributions from the Coulomb interaction at small momentum-transfer, capturing the effects of the strong Coulomb repulsion at the nonperturbative level. The contributions from the effective phonon-exchange interactions will be analyzed next, assessing their enhancement at low energies from the nontrivial scaling of the backscattering interaction channels.

On the other hand, we will pay also attention to the particular conditions in the experiment reported in Ref. 18. Each nanotube is embedded there in a large three-dimensional (3D) array of nanotubes. Thus, the electrostatic coupling between charges in the different nanotubes leads to a large screening of the Coulomb potential. We will study this effect by using a kind of generalized RPA scheme, taking into account the Coulomb interaction between all the nanotubes in the 3D array. We will show that, over distances much larger than the intertube separation, there is a regime where the nanotube array screens effectively as a 3D system, rendering short-ranged

the Coulomb potential within each nanotube. This is the most important effect of the environment in the particular experimental setup described in Ref. 18. We will see that the strong reduction of the Coulomb interaction leads then to the prevalence of charge instabilities with similar character to the Wentzel-Bardeen singularity²³.

We may compare the results of our investigation with those obtained for the small-diameter zigzag nanotubes by means of *ab initio* simulations²⁴ and mean-field-like calculations²⁵. In Ref. 25, a superconducting instability has been found to be dominant in the (5,0) nanotubes, at a scale of about 1 K. On the other hand, a CDW instability has been identified in the same geometry at room temperature in Ref. 24. Our results stress that the scale and the type of electronic instability are very sensitive to the degree of screening applied to the nanotubes. We will find indeed that single (5,0) nanotubes (with just some screening from nearby gates) undergo the breakdown of the Luttinger liquid regime in favor of a CDW modulation at low energies. This is quite different from the instability found in the 3D array of nanotubes. In either case, we will see that the onset of the electronic instability takes place at temperatures ranging from $T_c \sim 10^{-4}$ K up to $\sim 10^2$ K, depending on the dielectric constant of the environment.

II. LUTTINGER LIQUID APPROACH TO ELECTRONIC PROPERTIES

As a first approximation to the electronic properties of the small-diameter nanotubes, we begin our analysis by focusing on the effects of the strong Coulomb repulsion. This is the dominant interaction in scattering processes at low momentum-transfer. Following Ref. 11, we take the Coulomb potential in the wrapped geometry as

$$V_C(\mathbf{r} - \mathbf{r}') = \frac{e^2/\kappa}{\sqrt{(x - x')^2 + 4R^2 \sin^2[(y - y')^2/2R^2] + a_z^2}} \quad (1)$$

where $a_z \simeq 1.6$ Å and R is the nanotube radius. The effective strength of the interaction depends on the dielectric properties of the environment hosting the nanotubes. In general, we will encode the screening effects from external gates in the dielectric constant κ . We have to bare in mind, however, that this procedure is suitable for the description of single nanotubes, while it has to be appropriately improved for systems made of a manifold of nanotubes, as we will see in Sec. IV.

The Fourier transform $\tilde{V}_C(k, q)$ of the potential (1) reflects the long-range character of the interaction at small momentum-transfer. Thus, it has a logarithmic dependence at small longitudinal momentum k , which is characteristic of the 1D Coulomb potential in momentum space²⁶:

$$\tilde{V}_C(k, 0) \approx \frac{2e^2}{\kappa} \log\left(\frac{k_c + k}{k}\right), \quad (2)$$

k_c is in general of the order of the inverse of the nanotube radius R , as it is the memory that the electron system keeps of the finite transverse size, after projection of the 3D potential onto the longitudinal direction of the tubule. The strength of the Coulomb interaction can be estimated from the dimensionless ratio $e^2/\kappa v_F$, which for the small-diameter nanotubes is of the order of $\sim 8/\kappa$. This gives a measure of the relevance of the Coulomb interaction, which turns out to be in the strong-coupling regime in the forward-scattering channels.

Before going ahead, we proceed next to make a complete catalogue of the different interaction channels. We first borrow the classification that has been already made for metallic nanotubes with a pair of subbands at the Fermi level²⁰. Thus, we introduce respective coupling constants $g_i^{(j)}$ for the channels involving processes between the two inner subbands of the small-diameter nanotubes. The lower index discerns whether the interacting particles shift from one subband to the other ($i = 1$), remain at different subbands ($i = 2$), or they interact within the same subband ($i = 4$). The upper label follows the same rule to classify the different combinations of left-movers and right-movers.

The above set of couplings $g_i^{(j)}$ has to be supplemented with the couplings for the channels involving processes between a particle at one of the degenerate subbands and another at the nondegenerate subband. Now we can discern between interactions that keep each particle within its respective subband, to which we assign a coupling $f^{(2)}$ ($f^{(4)}$) for particles of opposite (like) chirality, and backscattering interactions that lead to the exchange of the subbands for the two particles, which we label with a coupling $f^{(1)}$. Moreover, we have also the channels in which the particles interact within the outer subband, and that we will label as in the usual *g*-ology description, in terms of the couplings $g^{(1)}$, $g^{(2)}$ and $g^{(4)}$. Finally, there are also interaction processes in which two particles with about zero total momentum exchange their position from the outer to the inner subbands, or vice versa, as depicted in Fig. 3. We will assign the coupling u_F to that kind of interaction with no change of chirality of the particles, and the coupling u_B when there is a change in their chirality. It is worthwhile to remark that, despite the role they may have in the enhancement of some type of correlations, these interactions labelled by u_F and u_B have been overlooked in previous studies of the (5,0) nanotubes²⁷.

Focusing again on the forward-scattering interactions, we may represent their contribution to the hamiltonian of the electron system introducing the charge and spin density operators

$$\rho_{ri}(x) = \frac{1}{\sqrt{2}}(\Psi_{ri\uparrow}^\dagger(x)\Psi_{ri\uparrow}(x) + \Psi_{ri\downarrow}^\dagger(x)\Psi_{ri\downarrow}(x)) \quad (3)$$

$$\sigma_{ri}(x) = \frac{1}{\sqrt{2}}(\Psi_{ri\uparrow}^\dagger(x)\Psi_{ri\uparrow}(x) - \Psi_{ri\downarrow}^\dagger(x)\Psi_{ri\downarrow}(x)) \quad (4)$$

which correspond to the different electron fields $\Psi_{ri\sigma}$ for the linear branches about the Fermi points shown in Fig.

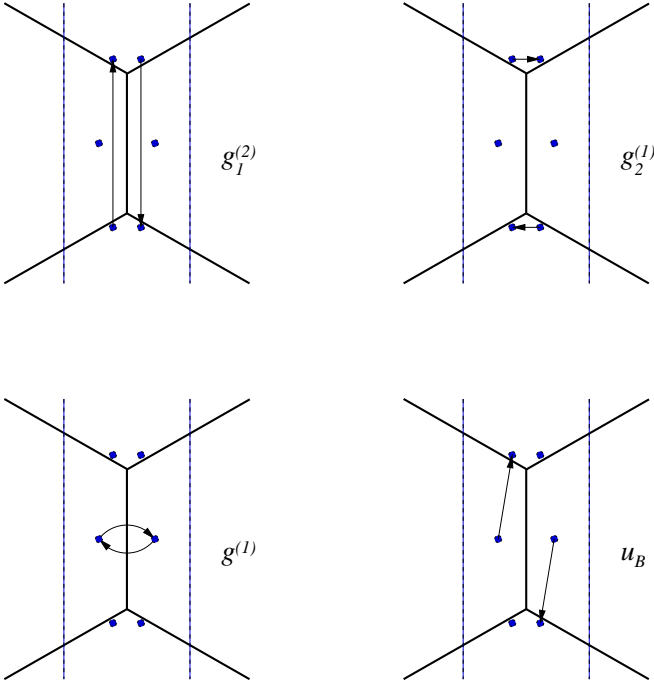


FIG. 3: Diagrams showing the shift in momentum space of the interacting electrons and the momentum-transfer involved in different backscattering processes in the (5,0) nanotubes.

2. We adopt a notation in which the index $r = L, R$ is used to label the left- or right-moving character of the linear branch, and the index $i = 0, 1, 2$ to label the subband. We will assume that the interaction mediated by phonon exchange (as well as the Coulomb interaction) does not depend on the spin of the interacting electrons, so that we will carry out the discussion in terms of the charge density operators.

For the sake of organizing the different forward-scattering interactions, it is convenient to define the symmetric and antisymmetric combinations of corresponding density operators in the two degenerate subbands:

$$\rho_{R\pm}(k) = \frac{1}{\sqrt{2}}(\rho_{R1}(k) \pm \rho_{R2}(k)) \quad (5)$$

$$\rho_{L\pm}(k) = \frac{1}{\sqrt{2}}(\rho_{L2}(k) \pm \rho_{L1}(k)). \quad (6)$$

With this change of variables, the hamiltonian for the forward-scattering interactions can be written in the form

$$\begin{aligned} H_{FS} = & \frac{1}{2}v_F \int_{-k_c}^{k_c} dk \sum_{r=L,R} \sum_{i=\pm} \rho_{ri}(k) \rho_{ri}(-k) \\ & + \frac{1}{2}v_F^{(0)} \int_{-k_c}^{k_c} dk \sum_{r=L,R} \rho_{r0}(k) \rho_{r0}(-k) \\ & + \frac{1}{2} \int_{-k_c}^{k_c} \frac{dk}{2\pi} 2 \left(\rho_{R+}(k) (g_4^{(4)} + g_2^{(4)}) \rho_{R+}(-k) \right. \\ & \left. + \rho_{L+}(k) (g_4^{(4)} + g_2^{(4)}) \rho_{L+}(-k) \right. \end{aligned}$$

$$\begin{aligned} & + \rho_{R-}(k) (g_4^{(4)} - g_2^{(4)}) \rho_{R-}(-k) \\ & + \rho_{L-}(k) (g_4^{(4)} - g_2^{(4)}) \rho_{L-}(-k) \\ & + 2\rho_{R+}(k) (g_4^{(2)} + g_2^{(2)}) \rho_{L+}(-k) \\ & + 2\rho_{R-}(k) (g_2^{(2)} - g_4^{(2)}) \rho_{L-}(-k) \Big) \\ & + \frac{1}{2} \int_{-k_c}^{k_c} \frac{dk}{2\pi} 2 \left(\rho_{R0}(k) g^{(4)} \rho_{R0}(-k) \right. \\ & + \rho_{L0}(k) g^{(4)} \rho_{L0}(-k) + 2\rho_{R0}(k) g^{(2)} \rho_{L0}(-k) \Big) \\ & + \frac{1}{2} \int_{-k_c}^{k_c} \frac{dk}{2\pi} 4\sqrt{2} \left(\rho_{R+}(k) f^{(4)} \rho_{R0}(-k) \right. \\ & + \rho_{L+}(k) f^{(4)} \rho_{L0}(-k) + \rho_{R+}(k) f^{(2)} \rho_{L0}(-k) \\ & \left. + \rho_{L+}(k) f^{(2)} \rho_{R0}(-k) \right), \quad (7) \end{aligned}$$

where k_c stands again for the momentum cutoff dictated by the transverse size of the nanotube.

In order to diagonalize the hamiltonian (7), we introduce the fields $\Phi_+(x), \Phi_-(x), \Phi_0(x)$ (and their respective conjugate momenta, $\Pi_+(x), \Pi_-(x), \Pi_0(x)$) having the following relation with the electron density operators:

$$\partial_x \Phi_+(x) = \sqrt{\pi}(\rho_{L+}(x) + \rho_{R+}(x)) \quad (8)$$

$$\partial_x \Phi_-(x) = \sqrt{\pi}(\rho_{L-}(x) + \rho_{R-}(x)) \quad (9)$$

$$\partial_x \Phi_0(x) = \sqrt{\pi}(\rho_{L0}(x) + \rho_{R0}(x)). \quad (10)$$

In terms of these fields, we can write the hamiltonian (7) in the form

$$\begin{aligned} H_{FS} = & \frac{1}{2}u_+ \int dx (K_+(\Pi_+(x))^2 + (1/K_+)(\partial_x \Phi_+(x))^2) \\ & + \frac{1}{2}u_- \int dx (K_-(\Pi_-(x))^2 + (1/K_-)(\partial_x \Phi_-(x))^2) \\ & + \frac{1}{2}u_0 \int dx (K_0(\Pi_0(x))^2 + (1/K_0)(\partial_x \Phi_0(x))^2) \\ & + \frac{1}{2} \int dx \frac{2\sqrt{2}}{\pi} \left(\Pi_+(x) (f^{(4)} - f^{(2)}) \Pi_0(x) \right. \\ & \left. + \partial_x \Phi_+(x) (f^{(4)} + f^{(2)}) \partial_x \Phi_0(x) \right). \quad (11) \end{aligned}$$

The renormalized velocities u_+, u_-, u_0 and charge stiffnesses K_+, K_-, K_0 are given by the equations

$$u_{\pm} K_{\pm} = v_F + (1/\pi) \left(g_4^{(4)} \pm g_2^{(4)} - (g_2^{(2)} \pm g_4^{(2)}) \right) \quad (12)$$

$$u_{\pm}/K_{\pm} = v_F + (1/\pi) \left(g_4^{(4)} \pm g_2^{(4)} + (g_2^{(2)} \pm g_4^{(2)}) \right) \quad (13)$$

$$u_0 K_0 = v_F^{(0)} + (1/\pi) \left(g^{(4)} - g^{(2)} \right) \quad (14)$$

$$u_0/K_0 = v_F^{(0)} + (1/\pi) \left(g^{(4)} + g^{(2)} \right). \quad (15)$$

At this stage, the hamiltonian (11) can be brought to diagonal form by: i) applying a simple canonical transformation

$$\Phi_+ = \sqrt{K_+} \tilde{\Phi}_+ \quad , \quad \Pi_+ = \frac{1}{\sqrt{K_+}} \tilde{\Pi}_+$$

$$\begin{aligned}\Phi_- &= \sqrt{K_-} \tilde{\Phi}_- \quad , \quad \Pi_- = \frac{1}{\sqrt{K_-}} \tilde{\Pi}_- \\ \Phi_0 &= \sqrt{K_0} \tilde{\Phi}_0 \quad , \quad \Pi_0 = \frac{1}{\sqrt{K_0}} \tilde{\Pi}_0\end{aligned}\quad (16)$$

and ii) making an additional rotation to disentangle the $(+, 0)$ sector:

$$\begin{aligned}\tilde{\Phi}_0 &= c_0 \sqrt{\mu} \hat{\Phi}_0 + s_0 \sqrt{\nu} \hat{\Phi}_+ \\ \tilde{\Pi}_0 &= \frac{c_0}{\sqrt{\mu}} \hat{\Pi}_0 + \frac{s_0}{\sqrt{\nu}} \hat{\Pi}_+ \\ \tilde{\Phi}_+ &= c_+ \sqrt{\beta} \hat{\Phi}_+ + s_+ \sqrt{\alpha} \hat{\Phi}_0 \\ \tilde{\Pi}_+ &= \frac{c_+}{\sqrt{\beta}} \hat{\Pi}_+ + \frac{s_+}{\sqrt{\alpha}} \hat{\Pi}_0,\end{aligned}\quad (17)$$

where the parameters $c_0, s_0, c_+, s_+, \alpha, \beta, \mu, \nu$ are evaluated in Appendix A. The important point is that, at the end, the excitations of the system governed by the hamiltonian (11) are given by charge fluctuations, with velocities strongly renormalized by the interactions, and which constitute the whole spectrum together with the spin fluctuations propagating with the unrenormalized velocities v_F and $v_F^{(0)}$.

The picture that we have just developed corresponds to the Luttinger liquid regime of the electron system, in which the main physical properties are given by the charge stiffnesses in the different sectors and by the velocities of the charge and spin fluctuations²². These parameters may be used, for instance, to characterize the compressibilities in the symmetric, antisymmetric and zero angular-momentum sectors, which turn out to be proportional to the respective charge stiffnesses.

The Luttinger liquid behavior in the carbon nanotubes holds at energies where there is approximate linear dispersion of the different subbands crossing the Fermi level. This places typically an upper scale E_c of the order of ~ 0.1 eV. In the case of single nanotubes, the dominant contribution to the forward-scattering couplings in (7) comes from the strong Coulomb potential in (2), with some infrared cutoff which is dictated in general by the longitudinal size of the nanotube¹¹. This leads to values of the charge stiffnesses that are typically smaller than 1 and in agreement with the experimental observations of Luttinger liquid behavior in the carbon nanotubes^{2,3}. For energy scales much lower than E_c , however, the rest of interaction channels neglected in the above analysis may become as important as the forward-scattering channels. This is possible as the strength of the 1D interactions depends in general on the energy scale of the interaction processes¹⁹. Electronic instabilities are then expected when some of the backscattering interactions leave the weak-coupling regime as the temperature or other relevant energy scale is lowered, as we analyze next in the case of the small-diameter (5,0) nanotubes.

III. BACKSCATTERING INTERACTIONS AND LOW-ENERGY INSTABILITIES

The small-diameter nanotubes are systems where the backscattering interactions may lead to a significant enhancement of the electronic instabilities. Due to the large curvature of the tubes, the electron-phonon couplings turn out to be much larger than for nanotubes of typical radius. This leads consequently to a larger electron-electron interaction mediated by the exchange of phonons. In the case of single nanotubes, this effective interaction is anyhow overcome by the strong Coulomb repulsion given by the potential (2) in the forward-scattering channels. The opposite situation is found however in the backscattering channels, as we discuss in what follows.

In general, the exchange of phonons between electronic currents gives rise to a retarded interaction, which can be represented by the effective potential obtained by integrating out the phonons in the many-body theory²³. If we denote the electron-phonon couplings by $g_{ii'}(k)$ (labelling by i, i' the subbands of the incoming and the outgoing electron), we can express the potential for the effective electron-electron interaction in the form

$$V_{ij, i' j'}(k, \omega) = -2g_{ii'}(k)g_{jj'}(-k) \frac{\omega_k}{-\omega^2 + \omega_k^2}, \quad (18)$$

where ω_k stands for the energy of the exchanged phonon with momentum k . The typical energy of the phonons in the optical branches (or in the acoustic branches at large momentum-transfer) is of the order of ~ 0.1 eV²⁵, and therefore comparable to the energy cutoff E_c of the 1D electron system. This allows us to take the interaction arising from (18) as a source of attraction, in the energy range where the 1D model makes sense.

The electron-phonon couplings in the (5,0) nanotubes have been analyzed with great detail in Ref. 25. It has been shown there that the couplings with greater strength correspond to intraband processes, for which the momentum-transfer is in the longitudinal direction. Following for instance the results of that reference for the backscattering processes within subband 1 (or subband 2), we find that the strength of the effective electron-electron interaction with $2k_F$ momentum-transfer is given by the coupling

$$\sum_{\nu} 2 \left(g_{11}^{(\nu)}(2k_F) \right)^2 / v_F \omega_{2k_F}^{(\nu)} \approx 0.6 \quad (19)$$

after summing over the different phonon modes with nonvanishing electron-phonon coupling²⁵. Similarly, for backscattering processes within the nondegenerate subband we find the effective coupling

$$\sum_{\nu} 2 \left(g_{00}^{(\nu)}(2k_F^{(0)}) \right)^2 / v_F \omega_{2k_F^{(0)}}^{(\nu)} \approx 1.1. \quad (20)$$

The first of these values represents the contribution of the attractive phonon-mediated interaction to the couplings $g_2^{(1)}$ and $g_4^{(1)}$, while the second value provides the

contribution to the coupling $g^{(1)}$. Making similar estimates of the electron-phonon couplings and frequencies at large transverse momentum-transfer, we have found that the couplings for the rest of backscattering interactions $g_1^{(1)}, g_1^{(2)}, f^{(1)}, u_F$ and u_B are given by $\approx 0.5v_F$.

To each of these backscattering contributions, one has to subtract an opposite correction from the Coulomb interaction. This is given by the Fourier transform $\tilde{V}_C(k, q)$ of the potential in (1) at the corresponding momentum-transfer, with an additional factor of reduction that comes from the particular structure of the Bloch functions in the small-diameter nanotubes²⁵. In general, the larger contributions from the Coulomb potential are found in the channels with the smaller momentum-transfer. The forward-scattering channels deserve special consideration, as the potential (2) has to be evaluated with a cutoff at small k . As already mentioned, this is provided in general by the length L of the experimental samples, so that a sensible estimate is given typically by a spatial average of the potential $\tilde{V}_C(k \approx 0, 0) \approx (2e^2/\kappa) \log(k_c/k_0)$, with $k_0 \sim 1/L \sim 10^{-3}k_c$.

In this section we analyze the instabilities of single nanotubes, so that we can disregard for the moment any kind of intertube interaction. Then, taking into account the contributions from the phonon-exchange and the Coulomb interaction, we obtain the following values for the couplings in the different interaction channels:

$$g_4^{(4)}/v_F = g_2^{(4)}/v_F = g_4^{(2)}/v_F = g_2^{(2)}/v_F \approx 100/\kappa \quad (21)$$

$$g^{(4)}/v_F = g^{(2)}/v_F = f^{(4)}/v_F = f^{(2)}/v_F \approx 100/\kappa \quad (22)$$

$$g_4^{(1)}/v_F = g_2^{(1)}/v_F \approx -0.6 + 3.6/\kappa \quad (23)$$

$$g^{(1)}/v_F \approx -1.1 + 1.1/\kappa \quad (24)$$

$$f^{(1)}/v_F = u_B/v_F \approx -0.5 + 0.5/\kappa \quad (25)$$

$$u_F/v_F \approx -0.5 + 0.3/\kappa \quad (26)$$

$$g_1^{(1)}/v_F = g_1^{(2)}/v_F \approx -0.5 + 0.05/\kappa \quad (27)$$

We note again that the different contributions from the Coulomb interaction (with a $1/\kappa$ reduction in each case) correspond to the pertinent choices of the momentum-transfer in the evaluation of $\tilde{V}_C(k, q)$.

The relevance of the backscattering interactions comes from the fact that they give rise to quantum corrections that depend logarithmically on the energy scale. In the case of the $g_2^{(1)}$ interaction, for instance, the bare coupling is corrected to second order by the diagrams shown in Fig. 4. By following the renormalization group program, we translate the logarithmic dependence on energy of the terms in the diagrammatic expansion into the scale-dependence of renormalized coupling constants¹⁹. Up to terms quadratic in the backscattering interactions, we find the complete set of scaling equations

$$\frac{\partial g_1^{(1)}}{\partial l} = -\frac{1}{\pi v_F} (g_1^{(1)} g_1^{(1)} + g_1^{(2)} g_2^{(1)}) - \frac{1}{\pi v_F} \beta u_F u_B \quad (28)$$

$$\frac{\partial g_1^{(2)}}{\partial l} = (1 - \frac{1}{K_-}) g_1^{(2)} - \frac{1}{\pi v_F} (g_2^{(1)} g_1^{(1)})$$

$$+ (\beta/2) (u_F^2 + u_B^2) \quad (29)$$

$$\frac{\partial g_2^{(1)}}{\partial l} = (1 - \frac{1}{K_-}) g_2^{(1)} - \frac{1}{\pi v_F} (2g_4^{(1)} g_2^{(1)} - g_4^{(1)} g_1^{(2)}) + g_1^{(2)} g_1^{(1)} + \beta u_F u_B \quad (30)$$

$$\frac{\partial g_2^{(2)}}{\partial l} = -\frac{1}{2\pi v_F} (g_2^{(1)} g_2^{(1)} + g_1^{(1)} g_1^{(1)} + g_1^{(2)} g_1^{(2)}) \quad (31)$$

$$\frac{\partial g_4^{(1)}}{\partial l} = -\frac{1}{\pi v_F} (g_4^{(1)} g_4^{(1)} + g_2^{(1)} g_2^{(1)} - g_1^{(2)} g_2^{(1)}) \quad (32)$$

$$\frac{\partial g_4^{(2)}}{\partial l} = -\frac{1}{2\pi v_F} (g_4^{(1)} g_4^{(1)} - g_1^{(2)} g_1^{(2)}) \quad (33)$$

$$\frac{\partial g^{(2)}}{\partial l} = -\frac{1}{\pi v_F} ((\beta/2) g^{(1)} g^{(1)} + u_F^2 + u_B^2) \quad (34)$$

$$\frac{\partial g^{(1)}}{\partial l} = -\frac{1}{\pi v_F} (\beta g^{(1)} g^{(1)} + 2u_F u_B) \quad (35)$$

$$\frac{\partial f^{(2)}}{\partial l} = -\frac{\alpha}{2\pi v_F} (f^{(1)} f^{(1)} - u_F^2) \quad (36)$$

$$\frac{\partial f^{(1)}}{\partial l} = -\frac{\alpha}{\pi v_F} (f^{(1)} f^{(1)} + u_B^2 - u_F u_B) \quad (37)$$

$$\frac{\partial u_F}{\partial l} = \Delta u_F - \frac{1}{2\pi v_F} (g_1^{(2)} u_F + (g_2^{(1)} + g_1^{(1)} + \beta g^{(1)}) u_B) \quad (38)$$

$$\frac{\partial u_B}{\partial l} = \Delta u_B - \frac{1}{2\pi v_F} (g_1^{(2)} u_B + (g_2^{(1)} + g_1^{(1)} + \beta g^{(1)}) u_F + \frac{\alpha}{\pi v_F} f^{(1)} (u_F - 2u_B)), \quad (39)$$

where $\beta = v_F/v_F^{(0)}$, $\alpha = 2/(1 + v_F^{(0)}/v_F)$ and the anomalous dimension Δ depends on K_+, K_-, K_0 and $f^{(2)}$ as shown in Appendix A. In the above equations, the variable l stands for minus the logarithm of the energy (temperature) scale measured in units of the high-energy scale E_c of the 1D model (of the order of ~ 0.1 eV).

The equations for the $g_i^{(j)}$ couplings correspond to those already written for a model with two subbands in Ref. 20. Here we have incorporated a nonperturbative improvement of the equations by writing the exact dependence of the anomalous dimensions on the forward-scattering couplings through the K_+, K_- and K_0 parameters. This is essential to deal with the strong-coupling regime of the forward-scattering interactions in the case of single small-diameter nanotubes. Another important novelty is that the equations for the couplings in the degenerate and the nondegenerate subband mix through the couplings u_F and u_B , which had been overlooked however in previous analyses of the (5,0) nanotubes.

In order to determine the electronic instabilities that may appear in single small-diameter nanotubes, we have solved the set of scaling equations (28)-(39), taking initial values for the couplings according to the above discussion. The essential point is that the scaling equations reflect the strong screening that the couplings undergo

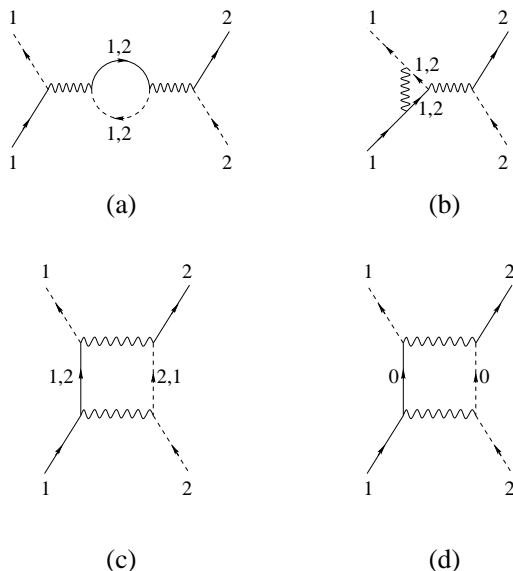


FIG. 4: Second-order diagrams with logarithmic dependence on the frequency renormalizing the $g_2^{(1)}$ interaction. The full (dashed) lines represent the propagation of electrons with right (left) chirality, and the wavy lines stand for the interactions. The labels 0,1,2 denote the respective low-energy subbands of the (5,0) nanotubes.

at low energies, which leads them to a regime of large attraction. To find the dominant instability in the electron system, one has to look at the behavior of the different response functions χ , which are catalogued in Appendix B. The regime of attraction leads to the large growth of some of the χ ; this points at a tendency towards long-range order, that cannot be completed anyhow at any finite frequency in the 1D system. The scaling of the interactions is cut off at some low-energy scale ω_c for which one of the charge stiffnesses β, μ or K_- diverges. We characterize the dominant instability by identifying the response function that reaches the largest value at the scale ω_c .

By varying the dielectric constant, we have found two different regimes, namely a regime characterized by the divergence of K_- (for $1 < \kappa < 1.6$ and $\kappa > 3.4$), and a regime with the divergence β (for $1.6 < \kappa < 3.4$). The largest growth for the response functions corresponds to χ_{CDW} , with large momentum connecting opposite Fermi points of the degenerate subbands (see Appendix B). We can understand this finding by looking at the competition between the phonon-exchange and Coulomb contributions in the different channels. At small κ , the couplings for large transverse momentum-transfer ($g_1^{(1)}, g_1^{(2)}$) are attractive from the very beginning (see Eq.(27)). In particular, the flow is dominated by $g_1^{(1)}$, which is driven to large attraction, leading to a rapid growth of χ_{CDW} .

Anyway, as shown in Fig.5, the χ_{CDW} grow large only for small values of κ ($\kappa \sim 1.4 \div 2$ for nanotubes in typical conditions). At large κ the maximum value for the all the response functions remain close to 10, signaling that

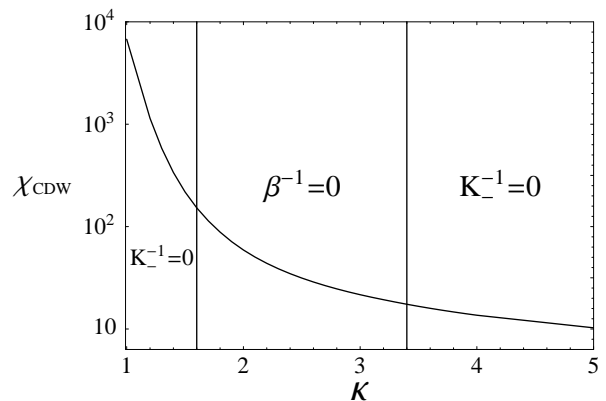


FIG. 5: Plot of $\chi_{CDW}(l_c)$ as a function of κ . Here $l_c = \log(E_c/\omega_c)$ is the scale at which the flow breaks down. The three regions with the corresponding divergent Luttinger liquid parameter are also indicated.

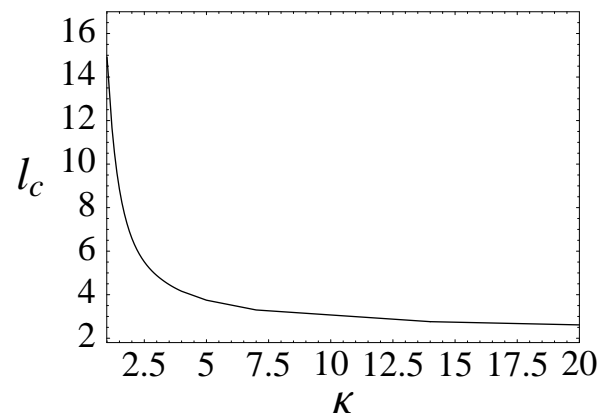


FIG. 6: Plot of minus the logarithm of the energy scale $l_c = \log(E_c/\omega_c)$ at which the flow breaks down, as a function of κ .

the tendency to ordering is weak.

In Fig.6 we have plotted the critical value $l_c = \log(E_c/\omega_c)$ at which the flow breaks down as a function of κ . It appears that the energy scale ω_c becomes quite sensitive to the value of the dielectric constant, implying that the onset of the electronic instability can be found at temperatures ranging from $T_c \sim 10^{-4}$ K (at $\kappa \approx 1$) up to a value $T_c \sim 10^2$ K (reached from $\kappa \approx 10$). Finally, we observe from the comparison in Fig. 7 that, while some charge and spin-density-wave response functions grow large by approaching the critical value l_c (at least for small κ), the superconducting response functions for different order parameters remain all small. This finding seems to rule out the possibility of having superconducting correlations in the (5,0) nanotubes, at least under the physical conditions considered in the present section.

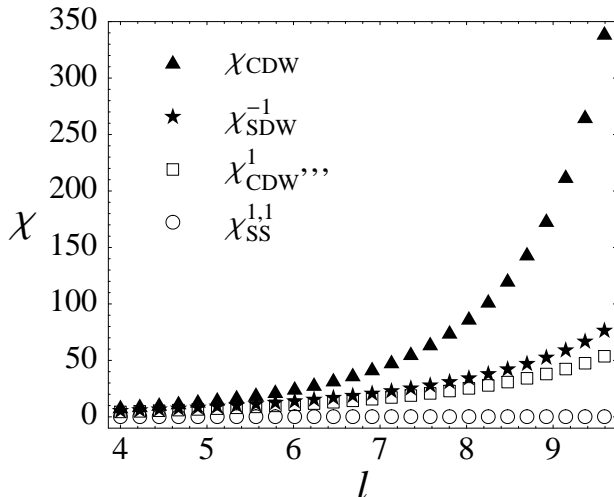


FIG. 7: Flow of the largest response functions (plus $\chi_{SS}^{1,1}$) at $\kappa = 1.4$.

IV. INTERTUBE SCREENING AND INSTABILITIES IN A 3D ARRAY OF NANOTUBES

While the above framework provides an accurate description of the instabilities of single small-diameter nanotubes, the analysis has to be conveniently modified when the electron system is composed of a manifold of nanotubes. This is the situation in the experiments reported in Ref. 18, where the samples contain large 3D arrays of small-diameter nanotubes. Systems that are formed by the assembly of a large amount of nanotubes, as is also the case of nanotube ropes, require in general an additional analysis of the interactions arising between different nanotubes. We will now focus on the conditions of the experimental samples studied in Ref. 18, which present a negligible intertube tunneling but have a significant coupling between electronic currents in different nanotubes.

Specifically, we will consider the case of an array of small-diameter nanotubes, arranged as a triangular lattice as viewed from a cross-section of the 3D array. We will denote by d the distance between nearest-neighbor nanotubes in such a lattice, having in mind that, for the samples studied in Ref. 18, its value is given by $d \approx 1$ nm. The coupling between different nanotubes at positions \mathbf{l} and \mathbf{l}' (measured in the cross-section of the array) comes from the Coulomb interaction, due to its long-range character. It may couple currents with large transverse separation $|\mathbf{l} - \mathbf{l}'|$ as long as the longitudinal momentum-transfer k becomes as small as $|\mathbf{l} - \mathbf{l}'|^{-1}$. The Coulomb potential $V_{\mathbf{l},\mathbf{l}'}(k)$ between currents in different nanotubes \mathbf{l} and \mathbf{l}' is actually obtained by partially Fourier-transforming the 3D Coulomb potential in the

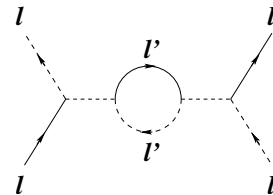


FIG. 8: Second-order process with logarithmic dependence on the frequency renormalizing intraband interactions at a given nanotube \mathbf{l} through the coupling with the nearest-neighbors \mathbf{l}' in a 3D array of nanotubes. The dashed lines (without arrow) stand for interactions between electronic currents in nearest-neighbor nanotubes.

longitudinal direction:

$$V_{\mathbf{l},\mathbf{l}'}(k) \approx \frac{2e^2}{\kappa} K_0(|\mathbf{l} - \mathbf{l}'|k), \quad (40)$$

$K_0(x)$ being the modified Bessel function, which diverges logarithmically as $x \rightarrow 0$ and is exponentially suppressed as for $x > 1$.

It is clear then that the nanotubes in the array may screen efficiently the forward-scattering interactions within each nanotube. This effect can be studied by extending the Random Phase Approximation (RPA) scheme to incorporate the electrostatic coupling between all the nanotubes in the array, as described in Appendix C. The main conclusion of this study is that the screened Coulomb potential $V_{\mathbf{l},\mathbf{l}}^{(r)}(k)$ within each nanotube becomes finite in the limit of vanishing momentum $k \rightarrow 0$, reaching a saturation value $V_{\mathbf{l},\mathbf{l}}^{(r)}(k=0) \approx 0.08e^2$. This corresponds to a dimensionless coupling $V_{\mathbf{l},\mathbf{l}}^{(r)}(k=0)/v_F \approx 0.65$, which is about two orders of magnitude smaller than the one for single nanotubes. In this case the phonon-exchange contribution competes with the Coulomb repulsion also in the intratube forward-scattering channels, changing qualitatively the physical picture.

One more important effect is that the coupling between currents in neighboring nanotubes may also correct the intratube backscattering interactions with small momentum-transfer. This is due to the fact that, for a longitudinal momentum-transfer $2k_F$, the Coulomb potential between nearest-neighbor nanotubes (such that $|\mathbf{l} - \mathbf{l}'| = d$) still has a nonnegligible strength, $V_{\mathbf{l},\mathbf{l}'}(2k_F) \approx 0.037e^2$. The important point is that this interaction gives rise to processes of the type depicted in Fig. 8, which depend on the energy scale and therefore introduce important renormalization effects for the intratube interactions at low energies. As observed from Fig. 8, the scaling analysis requires the definition of new backscattering interactions that couple electron currents in different nanotubes. We will assign the couplings $\tilde{g}_2^{(1)}$ and $\tilde{g}_4^{(1)}$ to the new channels represented in Figs. 9(a)-(b). As we are going to see next, these new couplings mix upon renormalization with two more channels corresponding to forward-scattering interactions between currents with

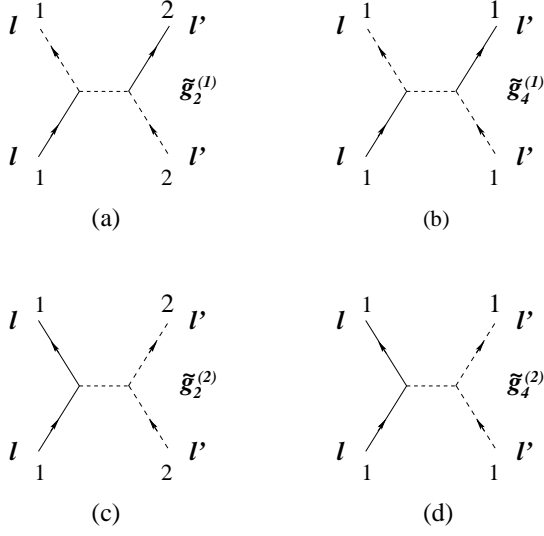


FIG. 9: Intertube interactions arising from the coupling between electronic currents in nearest-neighbor nanotubes I and I' of a 3D array. The meaning of the different lines is the same as in Figs. 4 and 8.

different chirality in nearest-neighbor nanotubes. These will be labelled by the couplings $\tilde{g}_4^{(2)}$ and $\tilde{g}_2^{(2)}$, as shown in Figs. 9(c)-(d).

In order to determine the perturbative scaling of the new intertube interactions $\tilde{g}_2^{(1)}$ and $\tilde{g}_4^{(1)}$, we pay attention to the second-order corrections that have logarithmic dependence on the energy scale. These have to be made of particle-particle processes or particle-hole loops with the nesting momenta $2k_F$ or $2k_F^{(0)}$. The different diagrams are shown in Fig. 10. We see that some of them involve the new intertube interactions $\tilde{g}_4^{(2)}$ and $\tilde{g}_2^{(2)}$. A consistent renormalization demands then the analysis of the scaling of this pair of couplings. This is dictated again by diagrams that depend logarithmically on the energy scale, depicted in Fig. 11 to second order in perturbation theory.

The main role of the intertube backscattering interactions $\tilde{g}_4^{(1)}$ and $\tilde{g}_2^{(1)}$ is to screen the intratube backscattering interactions through processes of the type shown in Fig. 8. Thus, the scaling equations for $g_2^{(1)}$ and $g_4^{(1)}$ get new contributions in the 3D array of nanotubes, taking now the form

$$\frac{\partial g_2^{(1)}}{\partial l} = \left(1 - \frac{1}{K_-}\right) g_2^{(1)} - \frac{1}{\pi v_F} (2g_4^{(1)} g_2^{(1)} - g_4^{(1)} g_1^{(2)}) + g_1^{(2)} g_1^{(1)} + \beta u_F u_B + 12\tilde{g}_4^{(1)} \tilde{g}_2^{(1)} \quad (41)$$

$$\frac{\partial g_4^{(1)}}{\partial l} = -\frac{1}{\pi v_F} (g_4^{(1)} g_4^{(1)} + g_2^{(1)} g_2^{(1)} - g_1^{(2)} g_2^{(1)}) + 6\tilde{g}_4^{(1)} \tilde{g}_4^{(1)} + 6\tilde{g}_2^{(1)} \tilde{g}_2^{(1)}. \quad (42)$$

We observe that the new terms are enhanced by a factor proportional to the number of nearest-neighbors of

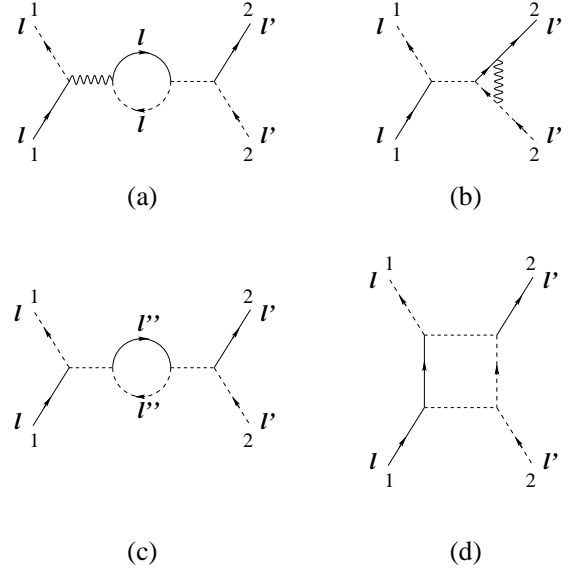


FIG. 10: Second-order diagrams with logarithmic dependence on the frequency renormalizing the intertube $\tilde{g}_2^{(1)}$ interaction. The wavy lines stand for intratube interactions and the dashed lines (without arrow) for interactions between nearest-neighbor nanotubes I, I' in a 3D array.

each nanotube in the 3D array. The scaling equations for the new intertube couplings follow from the diagrams depicted in Figs. 10 and 11:

$$\frac{\partial \tilde{g}_2^{(1)}}{\partial l} = -\frac{1}{\pi v_F} (2g_4^{(1)} \tilde{g}_2^{(1)} + 2g_2^{(1)} \tilde{g}_4^{(1)} + 4\tilde{g}_4^{(1)} \tilde{g}_2^{(1)} + \tilde{g}_2^{(2)} \tilde{g}_2^{(1)} - g_4^{(2)} \tilde{g}_2^{(1)} - g_1^{(2)} \tilde{g}_4^{(1)}) \quad (43)$$

$$\frac{\partial \tilde{g}_4^{(1)}}{\partial l} = -\frac{1}{\pi v_F} (2g_4^{(1)} \tilde{g}_4^{(1)} + 2g_2^{(1)} \tilde{g}_2^{(1)} + 2\tilde{g}_4^{(1)} \tilde{g}_4^{(1)} + 2\tilde{g}_2^{(1)} \tilde{g}_2^{(1)} + \tilde{g}_4^{(2)} \tilde{g}_4^{(1)} - g_4^{(2)} \tilde{g}_4^{(1)} - g_1^{(2)} \tilde{g}_2^{(1)}) \quad (44)$$

$$\frac{\partial \tilde{g}_4^{(2)}}{\partial l} = -\frac{1}{2\pi v_F} \tilde{g}_4^{(1)} \tilde{g}_4^{(1)} \quad (45)$$

$$\frac{\partial \tilde{g}_2^{(2)}}{\partial l} = -\frac{1}{2\pi v_F} \tilde{g}_2^{(1)} \tilde{g}_2^{(1)}. \quad (46)$$

Let us now discuss the initial conditions for the new set of scaling equations. The intratube backscattering couplings have the same initial values as in the preceding section since, according to the above discussion, the intertube screening in these channels is already incorporated in the scaling equations. Conversely, in the forward-scattering channels, the screening may be represented by finite diagrammatic corrections, which can be summed up with the RPA approach described in Appendix C. As mentioned before, the Coulomb contribution is given by the dimensionless coupling $\tilde{V}_{1,1}^{(r)}(k=0)/v_F \approx 0.65$. The phonon-exchange contribution at vanishing momentum-transfer can be estimated to be very similar to the value

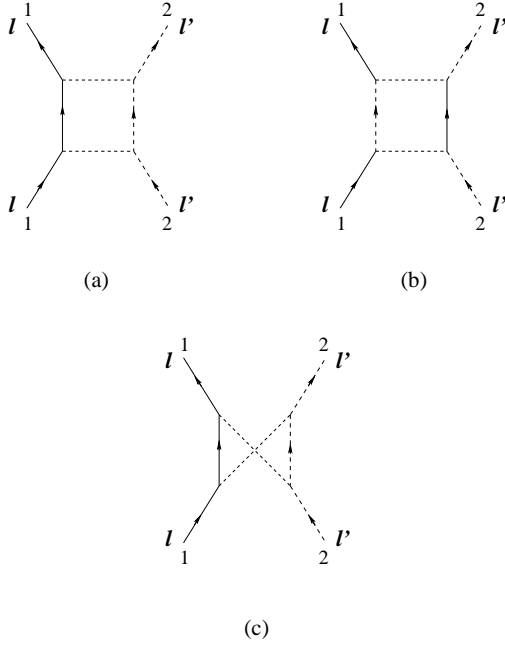


FIG. 11: Second-order diagrams with logarithmic dependence on the frequency renormalizing the intertube $\tilde{g}_2^{(2)}$ interaction. The dashed lines (without arrow) stand for interactions between nearest-neighbor nanotubes l, l' in a 3D array.

found from (19), showing that there is now a substantial suppression of the effects of the Coulomb repulsion in the intratube forward-scattering channels.

On the other hand, the intertube forward-scattering interactions are also screened due to the electrostatic coupling among the nanotubes in the array. These screening effects can be evaluated again within the RPA scheme in Appendix C, with the result that they render finite the intertube screened Coulomb potential at $k \rightarrow 0$. Furthermore, the values of the intertube backscattering couplings $\tilde{g}_2^{(1)}$ and $\tilde{g}_4^{(1)}$ can be obtained from (40) with $|l - l'| = d$. The new initial conditions obtained in this way read:

$$\tilde{g}_4^{(2)}/v_F = \tilde{g}_2^{(2)}/v_F \approx 0.002\kappa \quad (47)$$

$$\tilde{g}_2^{(1)}/v_F = \tilde{g}_4^{(1)}/v_F \approx 0.28/\kappa \quad (48)$$

We observe that the κ -dependence of the screened forward-scattering couplings is qualitatively different with respect to the unscreened interactions. In particular, we find that the intertube couplings have an approximate linear dependence on κ , at least up to $\kappa \sim 5$ (see Appendix C).

The numerical integration of the scaling equations shows now a new physical regime, where the instability of the system is not characterized by the large growth of any of the response functions, but only by the divergence of the charge stiffness β . We have plotted in Fig. 12 a typical flow of the dominant response functions up to the energy scale at which the divergence of the charge stiffness occurs. We note that the screening effects produced

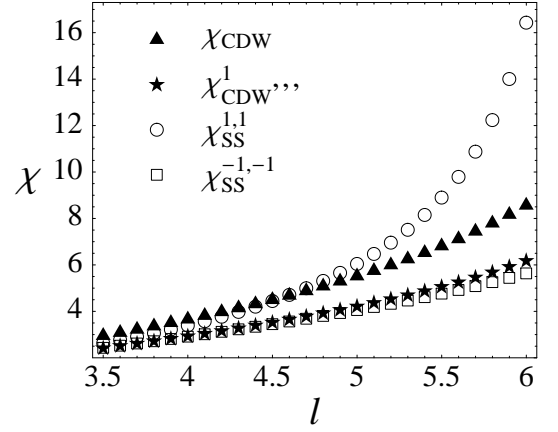


FIG. 12: Flow of the largest response functions at $\kappa = 2$.

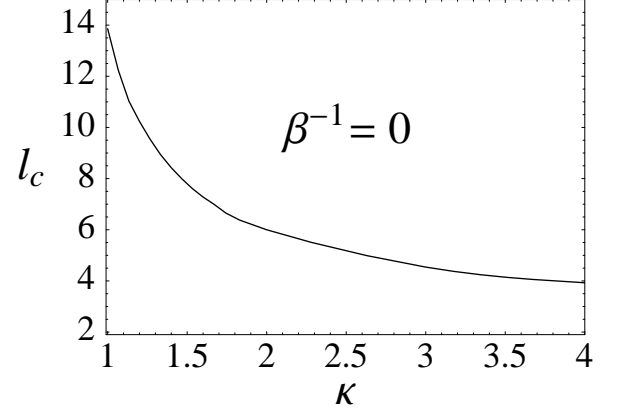


FIG. 13: Plot of minus the logarithm of the energy scale $l_c = \log(E_c/\omega_c)$ at which the flow breaks down, as a function of κ . The divergent Luttinger liquid parameter is also indicated.

by the environment of nanotubes suppress the tendency to CDW ordering, and enhance the superconducting correlations. Anyway, the values of $\chi_{SS}^{1,1}$ do not grow large, making very unlikely that they may give rise to any observable feature.

Otherwise, the divergence of β signals the onset of a regime of strong attraction, as it implies the divergence of the compressibility and density-density correlator in the corresponding sector and the vanishing of the renormalized Fermi velocity u_+/β as well. This points at the development of phase separation into spatial regions with different electronic density, in close analogy with the physical interpretation of the Wentzel-Bardeen singularity. The critical energy scale for this instability is shown in Fig. 13. For the zeolite matrix of Ref. 18, the estimate of the dielectric constant gives $\kappa \approx 2 \div 4$, which corresponds to a transition temperature $T_c \approx 3 \text{ K} \div 20 \text{ K}$, in qualitative agreement with the value $T_c \approx 15 \text{ K}$ observed experimentally.

V. CONCLUSION

In this paper we have studied the electronic instabilities of the small-diameter (5,0) nanotubes, by analyzing the competition between the Coulomb interaction and the effective interaction mediated by the exchange of phonons. We have built our framework on the basis that the Luttinger liquid is what characterizes the normal state of the carbon nanotubes. This is a key assumption, since the low-energy excitations of the 1D electron system are given in the normal state by charge and spin fluctuations, with absence of electron quasiparticles in the spectrum. This is consistent with the power-law suppression of the conductance and the differential conductivity that has been measured in several transport experiments on carbon nanotubes^{2,3,28}. The deviations from this picture have to be understood as perturbations of the Luttinger liquid behavior, which in general are nominally small as the strong Coulomb potential at small momentum-transfer provides the dominant interaction in the system.

There are however instances in which the enhancement of the backscattering interactions (corresponding to some nesting momentum between Fermi points) leads to the breakdown of the Luttinger liquid picture. This certainly happens at sufficiently small temperature, since the backscattering interactions are amplified at low energies until they reach the strong-coupling regime¹⁹. There are also experimental conditions in which the strong Coulomb repulsion is largely screened. The screening effects are particularly important when the nanotubes form large assemblies²⁹. This should explain for instance the appearance of a regime with superconducting correlations at low temperature in massive ropes. In this context, the increase in the curvature of the small-diameter nanotubes has to give rise to larger electron-phonon couplings¹⁶, implying in turn a natural enhancement of the backscattering interactions mediated by phonon-exchange. Thus, there have been good prospects to observe the effects of large electron correlations in the small-diameter nanotubes, specially in the (5,0) geometry which leads to a relatively large density of states at the Fermi level.

We have shown that the level of screening of the Coulomb interaction plays an important role in the development of the low-energy instabilities in the (5,0) nanotubes. In the case of single nanotubes exposed to the screening by external gates, the Luttinger liquid is unstable against the onset of a strong-coupling phase with very large CDW correlations. The temperature of crossover to the new phase depends crucially on the dielectric constant κ of the environment, ranging from $T_c \sim 10^{-4}$ K (at $\kappa \approx 1$) up to a value $T_c \sim 10^2$ K (reached from $\kappa \approx 10$). The inspection of the response functions measuring the superconducting correlations shows that these do not have an appreciable growth in the regime where the CDW correlations grow large. Thus, even under conditions of strong screening by external charges, the ob-

servation of any superconducting feature seems to be excluded in single nanotubes with the (5,0) geometry.

The physical picture is different when we consider the case of a large array of nanotubes, of the kind patterned by the channels of the zeolite matrix in the experiments of Ref. 18. The coupling between the nanotubes in the array leads to a large reduction of the Coulomb potential, which is rendered finite at vanishing momentum-transfer. The Coulomb interaction happens to be now in the weak-coupling regime, making therefore easier the destabilization of the Luttinger liquid. We have found however that, before the superconducting correlations may grow large, a singularity is reached in one of the charge stiffnesses of the Luttinger liquid. This implies the divergence of the compressibility in one of the charge sectors, and it has therefore the same physical interpretation as the Wentzel-Bardeen singularity²³. As the density-density correlator in each charge sector is proportional to the charge stiffness, the divergence of the latter leads to a phase where the system prefers to form electron aggregates, leaving some other regions with a defect of electron density. The possibility of a phase of this type has been already anticipated in Ref. 17. We have established that such a phase is realized under the particular experimental conditions reported in Ref. 18, prevailing over any superconducting instability at the transition temperatures found in our analysis.

The divergence of the charge stiffness opens the possibility of having a genuine phase transition in the (5,0) nanotubes, since the above breakdown of the Luttinger liquid takes place without the formation of long-range order in a continuous order parameter. We have seen that, for a choice of the dielectric constant in accordance with the experimental conditions described in Ref. 18, the transition temperature is of the same order as the temperature of the crossover to the pseudogap regime observed in that reference. It is worthwhile to stress that the divergence of the charge stiffness leads to the development of a pseudogap in the single-particle spectrum. The density of states near the Fermi level for electrons in subband i scales in the Luttinger liquid regime as

$$n_i(\varepsilon) \sim \varepsilon^{\alpha_i} \quad (49)$$

with α_i as given in Appendix A. Quite remarkably, the I - V characteristics reported in Ref. 18 show the evolution of the curves for decreasing temperature into a power-law behavior with an increasingly large exponent. This is in agreement with the prediction obtained from (49) when approaching the singularity in the charge stiffness. It becomes then plausible that the crossover to the pseudogap regime reported in Ref. 18 may correspond to the breakdown of the Luttinger liquid found in the present framework.

There are however other experimental features of the small-diameter nanotubes described in Ref. 18 that cannot be explained in terms of the electronic instabilities we have found in the present paper. The strong diamagnetic signal measured at low temperatures has been interpreted

in that reference as a consequence of entering a superconducting regime in the small-diameter nanotubes. It remains open the question of whether the armchair (3,3) nanotubes can be responsible for such a regime, or for some other type of electronic instability that may account for the strong diamagnetic signal, as some preliminary results seem to indicate³⁰. Other questions that deserve attention refer to the properties of the small-diameter nanotubes when eventually assembled into other aggregates different to those considered in the present paper. It may be interesting to see the influence of intertube tunneling between small-diameter nanotubes packed to form massive ropes. It will be crucial then to discern whether the zigzag (5,0) and the armchair (3,3) nanotubes lead to different phases, and whether they may support the appearance of larger superconducting correlations than those observed in massive ropes made of typical nanotubes.

Acknowledgements

The financial support of the Ministerio de Educación y Ciencia (Spain) through grant BFM2003-05317 is gratefully acknowledged. E. P. was also supported by INFN grant 10068.

Appendix A: Diagonalization of H_{FS} and evaluation of the anomalous dimensions

In this Appendix we diagonalize H_{FS} by means of a generalized Bogoliubov transformation. Since in Eq. (11) the $\{\Phi_-, \Pi_-\}$ sector is already decoupled, it is sufficient to operate the transformation by mixing only the $\hat{\Phi}_+, \hat{\Phi}_0$ fields and their corresponding conjugate momenta $\hat{\Pi}_+, \hat{\Pi}_0$. Therefore we introduce the new operators $\tilde{\hat{\Phi}}_+, \tilde{\hat{\Phi}}_0, \tilde{\hat{\Pi}}_+, \tilde{\hat{\Pi}}_0$ defined by:

$$\begin{aligned} \tilde{\hat{\Phi}}_0 &\equiv c_0 \sqrt{\mu} \hat{\Phi}_0 + s_0 \sqrt{\nu} \hat{\Phi}_+ \quad , \quad \tilde{\hat{\Pi}}_0 \equiv \frac{c_0}{\sqrt{\mu}} \hat{\Pi}_0 + \frac{s_0}{\sqrt{\nu}} \hat{\Pi}_+ \\ \tilde{\hat{\Phi}}_+ &\equiv c_+ \sqrt{\beta} \hat{\Phi}_+ + s_+ \sqrt{\alpha} \hat{\Phi}_0 \quad , \quad \tilde{\hat{\Pi}}_+ \equiv \frac{c_+}{\sqrt{\beta}} \hat{\Pi}_+ + \frac{s_+}{\sqrt{\alpha}} \hat{\Pi}_0, \end{aligned}$$

where $c_{0(+)} \equiv \cos \varphi_{0(+)}$ and $s_{0(+)} \equiv \sin \varphi_{0(+)}$ in order to ensure the standard commutation relations $[\hat{\Phi}_{0(+)}(x), \hat{\Pi}(x')_{0(+)}] = i\delta(x-x')$.

The angles φ_0, φ_+ and the parameters μ, ν, α, β depend on $K_0, K_+, u_0, u_+, f^{(2)}, f^{(4)}$, and must be determined by imposing that (i) $[\hat{\Phi}(x)_{0(+)}, \hat{\Pi}(x')_{+(0)}] = 0$, (ii) H_{FS} written in terms of the new fields gets diagonal, (iii) the coefficients of $(\partial_x \hat{\Phi}_{0(+)})^2$ and $(\hat{\Pi}_{0(+)})^2$ are the same. The corresponding algebraic system has an analytical solution in closed form under the condition $f^{(2)} = f^{(4)}$ ³¹:

$$\begin{aligned} \varphi_0 &= \frac{1}{2} \arctan \left(\frac{4\sqrt{2K_0K_+}f^{(2)}/\pi}{u_+^{3/2}/u_0^{1/2} - u_0^{3/2}/u_+^{1/2}} \right) \\ \varphi_+ &= -\varphi_0 \end{aligned}$$

$$\begin{aligned} \mu &= \left(c_0^2 + s_0^2 u_+^2 / u_0^2 - 4\sqrt{2K_0K_+}f^{(2)} c_0 s_0 u_+^{1/2} / \pi u_0^{3/2} \right)^{-1/2} \\ \beta &= \left(c_0^2 + s_0^2 u_0^2 / u_+^2 + 4\sqrt{2K_0K_+}f^{(2)} c_0 s_0 u_0^{1/2} / \pi u_+^{3/2} \right)^{-1/2} \\ \alpha &= \mu u_+ / u_0 \quad , \\ \nu &= \beta u_0 / u_+ \quad . \end{aligned}$$

The renormalized Fermi velocities of the new free-boson hamiltonian read:

$$\begin{aligned} u_+ &\rightarrow u_+ / \beta \quad , \\ u_0 &\rightarrow u_0 / \nu \quad . \end{aligned} \quad (50)$$

Now we use this result to calculate the nonperturbative contribution Δ to the scaling equations of u_F and u_B . For instance, let us focus on u_F , whose operator has the form

$$\begin{aligned} H_{u_F} &= u_F \sum_{\sigma, \sigma'} (\Psi_{R0\sigma}^\dagger \Psi_{R1\sigma} \Psi_{L0\sigma'}^\dagger \Psi_{L2\sigma'} + \\ &\quad \Psi_{R0\sigma}^\dagger \Psi_{R2\sigma} \Psi_{L0\sigma'}^\dagger \Psi_{L1\sigma'} + \text{h.c.}) \quad . \end{aligned} \quad (51)$$

The scaling dimension of H_{u_F} is readily evaluated with the bosonization technique, that allows us to express the fermion fields in terms of boson operators. For example let us bosonize one of the contributions to H_{u_F} :

$$\Psi_{R0}^\dagger \Psi_{R1} \Psi_{L0}^\dagger \Psi_{L2} \propto \exp \left[-\frac{i}{\sqrt{2}} (-\phi_{R0} + \phi_{R1} + \phi_{L0} - \phi_{L2}) \right] \quad .$$

Now we can read the anomalous dimension of this operator produced by the forward scattering interactions by expressing the boson fields ϕ in terms of the operators which diagonalize H_{FS} . The connection of the ϕ 's with the operators entering in the hamiltonian in Eq. (11) is given by:

$$\begin{aligned} \phi_{R1} &= \frac{1}{2\sqrt{2}} (\Phi_+ + \Phi_- + \theta_+ + \theta_-) \\ \phi_{R2} &= \frac{1}{2\sqrt{2}} (\Phi_+ - \Phi_- + \theta_+ - \theta_-) \\ \phi_{L1} &= \frac{1}{2\sqrt{2}} (\Phi_+ - \Phi_- - \theta_+ + \theta_-) \\ \phi_{L2} &= \frac{1}{2\sqrt{2}} (\Phi_+ + \Phi_- - \theta_+ - \theta_-) \\ \phi_{R0} &= \frac{1}{2} (\Phi_0 + \theta_0) \\ \phi_{L0} &= \frac{1}{2} (\Phi_0 - \theta_0) \quad , \end{aligned}$$

where the θ fields are related to the Π 's by:

$$\Pi_{\pm(0)} = -\partial_x \theta_{\pm(0)} \quad .$$

This allows us to write

$$\Psi_{R0}^\dagger \Psi_{R1} \Psi_{L0}^\dagger \Psi_{L2} \propto \exp \left[\frac{i}{\sqrt{2}} (\theta_0 - \frac{1}{\sqrt{2}} \theta_+ - \frac{1}{\sqrt{2}} \theta_-) \right]$$

$$= \exp \left[i\hat{\theta}_0 \left(\frac{c_0}{\sqrt{2K_0\mu}} + \frac{s_0}{2\sqrt{K_+\alpha}} \right) + i\hat{\theta}_+ \left(\frac{s_0}{\sqrt{2K_0\nu}} - \frac{c_0}{2\sqrt{K_+\beta}} \right) - i\hat{\Phi}_- \frac{1}{2\sqrt{K_-}} \right].$$

Finally the anomalous dimension Δ of the operator H_{u_F} is obtained by looking at the coefficients of the free fields in the exponent:

$$\Delta = 1 - \left(\frac{c_0}{\sqrt{2K_0\mu}} + \frac{s_0}{2\sqrt{K_+\alpha}} \right)^2 - \left(\frac{s_0}{\sqrt{2K_0\nu}} - \frac{c_0}{2\sqrt{K_+\beta}} \right)^2 - \left(\frac{1}{2\sqrt{K_-}} \right)^2.$$

By means of the same reasoning, we can compute also the anomalous dimensions of the operators $O_{\mu}^{P,Q}$ defining the two-particle correlation functions, introduced in Appendix B. They encode the nonperturbative corrections to the scaling Eqs. (53) for the response functions χ and read:

$$\Delta_{DW} = 1 - \frac{K_-}{2} - \frac{K_+}{2} (c_0^2\beta + s_0^2\alpha),$$

$$\Delta_{DW'} = 1 - \frac{1}{2K_-} - \frac{K_+}{2} (c_0^2\mu + s_0^2\nu),$$

$$\Delta_{DW''} = 1 - K_0 (c_0^2\mu + s_0^2\nu),$$

$$\Delta_{DW'''} = 1 - \frac{K_-}{8} - \frac{1}{8K_-} - 2 \left(\frac{\sqrt{K_+\beta}c_0}{4} + \frac{\sqrt{K_0\nu}s_0}{2\sqrt{2}} \right)^2 -$$

$$2 \left(\frac{\sqrt{K_0\mu}c_0}{2\sqrt{2}} - \frac{\sqrt{K_+\alpha}s_0}{4} \right)^2 - 2 \left(\frac{c_0}{4\sqrt{K_+\beta}} - \frac{s_0}{2\sqrt{2}\sqrt{K_0\nu}} \right)^2$$

$$- 2 \left(\frac{s_0}{4\sqrt{K_+\alpha}} + \frac{c_0}{2\sqrt{2}\sqrt{K_0\mu}} \right)^2,$$

$$\Delta_{SC}^{(a)} = 1 - \frac{1}{2K_-} - \frac{1}{2K_+} \left(\frac{c_0^2}{\beta} + \frac{s_0^2}{\alpha} \right),$$

$$\Delta_{SC}^{(b)} = 1 - \frac{1}{K_0} \left(\frac{c_0^2}{\mu} + \frac{s_0^2}{\nu} \right),$$

$$\Delta_{SC'} = 1 - \frac{K_-}{2} - \frac{1}{2K_+} \left(\frac{c_0^2}{\mu} + \frac{s_0^2}{\nu} \right),$$

$$\Delta_{SC''} = 1 - \frac{K_-}{8} - \frac{1}{8K_-} - 2 \left(\frac{\sqrt{K_+\beta}c_0}{4} - \frac{\sqrt{K_0\nu}s_0}{2\sqrt{2}} \right)^2 -$$

$$2 \left(\frac{\sqrt{K_0\mu}c_0}{2\sqrt{2}} + \frac{\sqrt{K_+\alpha}s_0}{4} \right)^2 - 2 \left(\frac{c_0}{4\sqrt{K_+\beta}} + \frac{s_0}{2\sqrt{2}\sqrt{K_0\nu}} \right)^2$$

$$- 2 \left(\frac{s_0}{4\sqrt{K_+\alpha}} - \frac{c_0}{2\sqrt{2}\sqrt{K_0\mu}} \right)^2.$$

Finally we evaluate the anomalous dimensions α_i governing the density of states near the Fermi level for elec-

trons in the different subbands $i = 0, 1, 2$, in the Luttinger liquid regime:

$$\alpha_1 = \alpha_2 = \frac{1}{8} [K_+ (c_0^2\beta + s_0^2\alpha) + \frac{1}{K_+} \left(\frac{c_0^2}{\beta} + \frac{s_0^2}{\alpha} \right) + K_- + \frac{1}{K_-} - 4],$$

$$\alpha_0 = \frac{1}{4} \left[K_0 (c_0^2\mu + s_0^2\nu) + \frac{1}{K_0} \left(\frac{c_0^2}{\mu} + \frac{s_0^2}{\nu} \right) - 2 \right].$$

Appendix B: Scaling equations for the response functions

In order to study the competition between the possible instabilities, one has to consider the scaling flow of the two-particle correlation functions χ . They measure the strength of the quantum fluctuations for a given type of ordering induced by the pair-field $O_{\mu}^{P,Q}$, in such a way that

$$\chi_{\mu}^{P,Q}(k, \omega_m) = - \int_0^{\beta} \int_0^L d\tau dx e^{ikx - i\omega_m\tau} \times \langle O_{\mu}^{P,Q}(x, \tau)^{\dagger} O_{\mu}^{P,Q}(0, 0) \rangle, \quad (52)$$

where L is the length of the nanotube, ω_m is the bosonic Matsubara frequency and $P, Q = \pm 1$ take into account the band-entanglement³². By neglecting the dependence on ω_m and expressing the momenta according to Fig.(14), the complete collection of the Fourier transforms of the response functions reads:

$$O_{DW, \mu}^P(k \approx 2k_{FL_2}) = \frac{1}{2\sqrt{L}} \sum_{p, \alpha, \beta} \left[\Psi_{R1\alpha}^{\dagger}(p-k) \sigma_{\mu}^{\alpha, \beta} \Psi_{L2\beta}(p) + P \Psi_{L1\alpha}^{\dagger}(p-k) \sigma_{\mu}^{\alpha, \beta} \Psi_{R2\beta}(p) \right],$$

$$O_{DW', \mu}^P(k \approx 2k_F) = \frac{1}{2\sqrt{L}} \sum_{p, \alpha, \beta} \left[\Psi_{R1\alpha}^{\dagger}(p-k) \sigma_{\mu}^{\alpha, \beta} \Psi_{L1\beta}(p) + P \Psi_{R2\alpha}^{\dagger}(p-k) \sigma_{\mu}^{\alpha, \beta} \Psi_{L2\beta}(p) \right],$$

$$O_{DW'', \mu}(k \approx 2k_F^{(0)}) = \frac{1}{\sqrt{L}} \sum_{p, \alpha, \beta} \left[\Psi_{R0\alpha}^{\dagger}(p-k) \sigma_{\mu}^{\alpha, \beta} \Psi_{L0\beta}(p) \right],$$

$$O_{DW''', \mu}^P(k \approx k_{FL_0} - k_{FR_1}) = \frac{1}{2\sqrt{L}} \sum_{p, \alpha, \beta} \left[\Psi_{R1\alpha}^{\dagger}(p-k) \sigma_{\mu}^{\alpha, \beta} \Psi_{L0\beta}(p) + P \Psi_{R0\alpha}^{\dagger}(p-k) \sigma_{\mu}^{\alpha, \beta} \Psi_{L2\beta}(p) \right],$$

$$O_{SC, \mu}^{P,Q}(k \approx 0) = \frac{1}{\sqrt{3L}} \sum_{p, \alpha, \beta} \left[\Psi_{R1\alpha}(-p+k) \sigma_{\mu}^{\alpha, \beta} \Psi_{L2\beta}(p) + P \Psi_{R2\alpha}(-p+k) \sigma_{\mu}^{\alpha, \beta} \Psi_{L1\beta}(p) + Q \Psi_{R0\alpha}(p-k) \sigma_{\mu}^{\alpha, \beta} \Psi_{L0\beta}(p) \right],$$

$$O_{SC', \mu}(k \approx k_{FR_1} + k_{FL_1}) = \frac{1}{\sqrt{L}} \sum_{p, \alpha, \beta} \left[\Psi_{R1\alpha}(-p+k) \sigma_{\mu}^{\alpha, \beta} \Psi_{L1\beta}(p) \right],$$

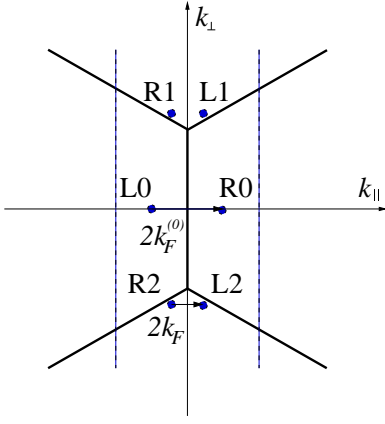


FIG. 14: Sketch of the Brillouin Zone of the (5,0) nanotube: the six Fermi points are indicated with the labels of corresponding chirality and subband. The longitudinal momentum transfers $2k_F$ and $2k_F^{(0)}$ are also drawn.

$$O_{SC'',\mu}(k \approx k_{FR1} + k_{FL0}) = \frac{1}{\sqrt{L}} \sum_{p,\alpha,\beta} [\Psi_{L0\alpha}(-p+k)\sigma_{\mu}^{\alpha,\beta}\Psi_{R1\beta}(p)] ,$$

where for density wave (DW) operators $\mu = 0$ stands for CDW and $\mu = 1, 2, 3$ for SDW; while for superconducting (SC) operators $\mu = 0$ stands for SS and $\mu = 1, 2, 3$ for TS; $\sigma_{\mu}^{\alpha,\beta}$ are the Pauli matrices, with $\sigma_0^{\alpha,\beta} = \mathbf{1}_{2 \times 2}$.

The response functions χ defined in Eq. (52) do not obey scaling equations¹⁹, but the auxiliary functions defined as $\bar{\chi}(k, l) = \pi v_F (d/dl)\chi(k, l)$ do. Finally the scaling equations for the $\bar{\chi}$ functions read:

$$\begin{aligned} \frac{\partial}{\partial l} \ln \bar{\chi}_{CDW} &= \Delta_{DW} - \frac{2}{\pi v_F} g_1^{(1)} , \\ \frac{\partial}{\partial l} \ln \bar{\chi}_{SDW} &= \Delta_{DW} , \\ \frac{\partial}{\partial l} \ln \bar{\chi}_{CDW'}^P &= \Delta_{DW'} - \frac{2}{\pi v_F} 2g_4^{(1)} + \frac{P}{\pi v_F} (g_1^{(2)} - 2g_2^{(1)}) , \\ \frac{\partial}{\partial l} \ln \bar{\chi}_{SDW'}^P &= \Delta_{DW'} + \frac{P}{\pi v_F} g_1^{(2)} , \\ \frac{\partial}{\partial l} \ln \bar{\chi}_{CDW''} &= \Delta_{DW''} - \frac{2\beta}{\pi v_F} g^{(1)} , \\ \frac{\partial}{\partial l} \ln \bar{\chi}_{SDW''} &= \Delta_{DW''} , \\ \frac{\partial}{\partial l} \ln \bar{\chi}_{CDW'''}^P &= \Delta_{DW'''} - \frac{2\alpha}{\pi v_F} f^{(1)} + \frac{\alpha P}{\pi v_F} (u_F - 2u_B) , \\ \frac{\partial}{\partial l} \ln \bar{\chi}_{SDW'''}^P &= \Delta_{DW'''} + \frac{\alpha P}{\pi v_F} u_F , \\ \frac{\partial}{\partial l} \ln \bar{\chi}_{SS}^{P,Q} &= \frac{2}{3} \Delta_{SC}^{(a)} + \frac{1}{3} \Delta_{SC}^{(b)} \\ &+ \frac{2}{3\pi v_F} [-g_1^{(1)} - P(g_1^{(2)} + g_2^{(1)})] \\ &- \frac{\beta}{3\pi v_F} [2(Q + PQ)(u_F + u_B) + g^{(1)}] , \end{aligned}$$

$$\begin{aligned} \frac{\partial}{\partial l} \ln \bar{\chi}_{TS}^{P,Q} &= \frac{2}{3} \Delta_{SC}^{(a)} + \frac{1}{3} \Delta_{SC}^{(b)} \\ &+ \frac{2}{3\pi v_F} [g_1^{(1)} - P(g_1^{(2)} - g_2^{(1)})] \\ &- \frac{\beta}{3\pi v_F} [2(Q + PQ)(u_F - u_B) - g^{(1)}] , \\ \frac{\partial}{\partial l} \ln \bar{\chi}_{SS'} &= \Delta_{SC'} - \frac{1}{\pi v_F} g_4^{(1)} , \\ \frac{\partial}{\partial l} \ln \bar{\chi}_{TS'} &= \Delta_{SC'} + \frac{1}{\pi v_F} g_4^{(1)} , \\ \frac{\partial}{\partial l} \ln \bar{\chi}_{SS''} &= \Delta_{SC''} - \frac{\alpha}{\pi v_F} f^{(1)} , \\ \frac{\partial}{\partial l} \ln \bar{\chi}_{TS''} &= \Delta_{SC''} + \frac{\alpha}{\pi v_F} f^{(1)} , \end{aligned} \quad (53)$$

where the nonperturbative contributions encoded in the anomalous dimensions $\Delta_{DW}, \Delta_{DW'}, \Delta_{DW''}, \Delta_{DW'''}, \Delta_{SC}^{(a,b)}, \Delta_{SC'}, \Delta_{SC''}$ are evaluated in Appendix A.

Appendix C: Intertube screening for forward scattering processes

In this Appendix we study the Coulomb interaction at small momentum-transfer between electrons belonging to different nanotubes in a 3D array. The long-range intertube effects operate in two ways: *i*) it provides a screening of the bare intratube forward-scattering couplings $g_2^{(2)}, g_2^{(4)}, g_4^{(2)}, g_4^{(4)}, g^{(2)}, g^{(4)}, f^{(2)}, f^{(4)}$, and *ii*) produces new intertube couplings $\tilde{g}_2^{(2)}, \tilde{g}_4^{(2)}$ (see Eqs. (45), (46)) with nontrivial scaling flow. Here we take into account the screening effects by the nanotube environment by generalizing the approach devised in Ref. 33, which essentially consists on a RPA treatment of the dielectric constant. The RPA approximation is justified as long as the electrons are not allowed to tunnel between different nanotubes, and we assume that this condition applies to the system under consideration in the main body of the paper. It is important to stress that the screened interactions obtained by this approach do not contain any dependence on the energy cutoff. As a consequence, the RPA screening only imposes the initial value of the forward-scattering couplings in Section IV, but does not affect their scaling flow.

Let \mathbf{l} and \mathbf{l}' be the positions of two nanotubes measured over a section of the 3D array, orthogonal to the tube axes. We introduce the long-range bare Coulomb interaction with momentum-transfer k along the longitudinal direction by partially Fourier-transforming the 3D Coulomb potential:

$$V_{\mathbf{l},\mathbf{l}'}(k) = \frac{2e^2}{\kappa} K_0(k|\mathbf{l} - \mathbf{l}'|) , \quad (54)$$

where $K_0(x)$ is the modified Bessel function, which diverges logarithmically as $x \rightarrow 0$ and is exponentially suppressed for $x > 1$. It is worth to observe that $V_{\mathbf{l},\mathbf{l}'}(k)$

does not take into account the variation of the electronic Bloch wavefunctions around the waist of the nanotubes. This approximation is justified as long as the transverse momentum-transfer is small, i.e. for forward-scattering processes. When $V_{1,I'}(k)$ is evaluated within the same nanotube, it is understood that $|\mathbf{I} - \mathbf{I}'| \sim R$, and we recover the intratube interaction of Eq. (2), with the logarithmic divergence at small momentum-transfer.

The RPA-screened $V_{1,I'}^{(r)}(k)$ obeys the Dyson equation

$$V_{1,I'}^{(r)}(k) = V_{1,I'}(k) + \Pi \sum_{I''} V_{1,I''}(k) V_{I'',I'}^{(r)}(k), \quad (55)$$

where I'' runs over all the positions of the nanotubes in the 3D array and Π is the polarizability of the 1D electron gas; its zero-frequency Fourier transform reads

$$\Pi(k) = \frac{2}{L} \sum_q \frac{f(\varepsilon_{q+k}) - f(\varepsilon_q)}{\varepsilon_{q+k} - \varepsilon_q}, \quad (56)$$

where f is the Fermi-Dirac distribution and L is the length of the nanotubes. In order to solve Eq. (55), we introduce the 2D Fourier transforms of $V_{1,I'}(k)$ and $V_{1,I'}^{(r)}(k)$:

$$V_{1,I'}(k) = \left(\frac{d}{2\pi}\right)^2 \int_{BZ} d^2\mathbf{p} \phi(k, \mathbf{p}) e^{i\mathbf{p}\cdot(\mathbf{I}-\mathbf{I}')}, \quad (57)$$

and the same with $V \rightarrow V^{(r)}$ and $\phi \rightarrow \phi^{(r)}$, where BZ indicates the first Brillouin zone of the nanotube lattice in the cross-section of the array, with lattice constant

$d \sim 1$ nm. In terms of $\phi(k, \mathbf{p})$ and $\phi^{(r)}(k, \mathbf{p})$, the Dyson equation reduces to

$$\phi^{(r)}(k, \mathbf{p}) = \phi(k, \mathbf{p}) + \Pi(k) \phi(k, \mathbf{p}) \phi^{(r)}(k, \mathbf{p}). \quad (58)$$

This permits to calculate the screened forward-scattering interaction with longitudinal momentum-transfer k between electrons in tubes at \mathbf{I} and \mathbf{I}' :

$$V_{1,I'}^{(r)}(k) = \left(\frac{d}{2\pi}\right)^2 \int_{BZ} d^2\mathbf{p} \frac{\phi(k, \mathbf{p})}{1 - \Pi(k)\phi(k, \mathbf{p})} e^{i\mathbf{p}\cdot(\mathbf{I}-\mathbf{I}')}. \quad (59)$$

The numerical evaluation of $V_{1,I'}^{(r)}(k)$ shows that such interaction is not negligible only for $\mathbf{I} = \mathbf{I}'$ and for nearest-neighbor tubes, i.e. for $|\mathbf{I} - \mathbf{I}'| = d$. This calls for the introduction of intertube couplings with $|\mathbf{I} - \mathbf{I}'| = d$. As discussed in Section IV, two of them ($\tilde{g}_2^{(2)}$ and $\tilde{g}_4^{(2)}$) have nontrivial scaling flow, and affect also the scaling of the intratube couplings.

The logarithmic divergence of $V_{1,I'}(k)$ at $k = 0$ is cured by the RPA screening; nevertheless the effective interactions are still enhanced at small k , but they saturate at a finite value. For the intratube interaction we have found that the saturation value is essentially independent on κ and is $V_{1,I'}^{(r)}(k=0)/v_F \approx 0.65$. In the intertube case, the RPA screening is much more efficient and the saturation value for $|\mathbf{I} - \mathbf{I}'| = d$ is $V_{1,I'}^{(r)}(k=0)/v_F \approx 0.002\kappa$, with an approximate linear dependence on κ , at least up to $\kappa \sim 5$. As discussed above, these asymptotic values are used as initial conditions for the forward-scattering couplings in the scaling equations in Section IV.

-
- ¹ R. Saito, M. Fujita, G. Dresselhaus and M. S. Dresselhaus, Appl. Phys. Lett. **60**, 2204 (1992). J. W. Mintmire, B. I. Dunlap and C. T. White, Phys. Rev. Lett. **68**, 631 (1992). N. Hamada, S. Sawada and A. Oshiyama, Phys. Rev. Lett. **68**, 1579 (1992).
- ² Z. Yao, H. W. Ch. Postma, L. Balents and C. Dekker, Nature **402**, 273 (1999).
- ³ M. Bockrath, D. H. Cobden, J. Lu, A. G. Rinzler, R. E. Smalley, L. Balents and P. L. McEuen, Nature **397**, 598 (1999).
- ⁴ A. Yu. Kasumov, R. Deblock, M. Kociak, B. Reulet, H. Bouchiat, I. I. Khodos, Yu. B. Gorbatov, V. T. Volkov, C. Journet and M. Burghard, Science **284**, 1508 (1999).
- ⁵ A. F. Morpurgo, J. Kong, C. M. Marcus and H. Dai, Science **286**, 263 (1999).
- ⁶ J. González, Phys. Rev. Lett. **87**, 136401 (2001).
- ⁷ M. Kociak, A. Yu. Kasumov, S. Guéron, B. Reulet, I. I. Khodos, Yu. B. Gorbatov, V. T. Volkov, L. Vaccarini and H. Bouchiat, Phys. Rev. Lett. **86**, 2416 (2001).
- ⁸ A. Kasumov, M. Kociak, M. Ferrier, R. Deblock, S. Guéron, B. Reulet, I. Khodos, O. Stéphan and H. Bouchiat, Phys. Rev. B **68**, 214521 (2003).
- ⁹ J. González, Phys. Rev. Lett. **88**, 076403 (2002); Phys. Rev. B **67**, 014528 (2003).
- ¹⁰ L. Balents and M. P. A. Fisher, Phys. Rev. B **55**, R11973 (1997).
- ¹¹ R. Egger and A. O. Gogolin, Phys. Rev. Lett. **79**, 5082 (1997); Eur. Phys. J. B **3**, 281 (1998).
- ¹² C. Kane, L. Balents and M. P. A. Fisher, Phys. Rev. Lett. **79**, 5086 (1997).
- ¹³ H. Yoshioka and A. A. Odintsov, Phys. Rev. Lett. **82**, 374 (1999); Phys. Rev. B **59**, R10457 (1999).
- ¹⁴ A. A. Nersesyan and A. M. Tselvelik, Phys. Rev. B **68**, 235419 (2003).
- ¹⁵ J. V. Alvarez and J. González, Phys. Rev. Lett. **91**, 076401 (2003).
- ¹⁶ L. X. Benedict, V. H. Crespi, S. G. Louie and M. L. Cohen, Phys. Rev. B **52**, 14935 (1995).
- ¹⁷ A. De Martino and R. Egger, Phys. Rev. B **67**, 235418 (2003).
- ¹⁸ Z. K. Tang, L. Zhang, N. Wang, X. X. Zhang, G. H. Wen, G. D. Li, J. N. Wang, C. T. Chan and P. Sheng, Science **292**, 2462 (2001).
- ¹⁹ J. Sólyom, Adv. Phys. **28**, 201 (1979).
- ²⁰ Yu. A. Krotov, D.-H. Lee and S. G. Louie, Phys. Rev. Lett. **78**, 4245 (1997).
- ²¹ R. Egger and H. Grabert, Phys. Rev. Lett. **79**, 3463 (1997).
- ²² V. J. Emery, in *Highly Conducting One-Dimensional Solids*, ed. J. T. Devreese, R. P. Evrard and V. E. Van Doren (Plenum, New York, 1979).

- ²³ D. Loss and T. Martin, Phys. Rev. B **50**, 12160 (1994).
- ²⁴ D. Connétable, G.-M. Rignanese, J.-C. Charlier and X. Blase, Phys. Rev. Lett. **94**, 015503 (2005).
- ²⁵ R. Barnett, E. Demler and E. Kaxiras, Phys. Rev. B **71**, 035429 (2005).
- ²⁶ D. W. Wang, A. J. Millis and S. Das Sarma, Phys. Rev. B **64**, 193307 (2001).
- ²⁷ K. Kamide, T. Kimura, M. Nishida and S. Kurihara, Phys. Rev. B **68**, 024506 (2003).
- ²⁸ A. Bachtold, M. de Jonge, K. Grove-Rasmussen, P. L. McEuen, M. Buitelaar and C. Schönberger, Phys. Rev. Lett. **87**, 166801 (2001).
- ²⁹ J. González, Eur. Phys. J. B **36**, 317 (2003).
- ³⁰ J. González, Phys. Rev. B (in press).
- ³¹ This condition is satisfied with great approximation in the systems considered in the paper, as the couplings $f^{(2)}$ and $f^{(4)}$ have equal values at the beginning of the scaling flow and they are very softly renormalized at low temperatures.
- ³² A. Sédéki, L. G. Caron and C. Bourbonnais, Phys. Rev. B **65**, 140515 (2002).
- ³³ P. Hawrylak, G. Eliasson and J. J. Quinn, Phys. Rev. B **37**, 10187 (1988).